RESEARCH ARTICLE | AUGUST 21 2013

High-performance symmetric electrochemical capacitor based on graphene foam and nanostructured manganese oxide

Abdulhakeem Bello; Omobosede O. Fashedemi; Joel N. Lekitima; Mopeli Fabiane; David Dodoo-Arhin; Kenneth I. Ozoemena; Yury Gogotsi; Alan T. Charlie Johnson; Ncholu Manyala

AIP Advances 3, 082118 (2013)
https://doi.org/10.1063/1.4819270

High-performance symmetric electrochemical capacitor based on graphene foam and nanostructured manganese oxide

Abdulhakeem Bello,[1] Omobosede O. Fashedemi,[2] Joel N. Lekitima,[2] Mopeli Fabiane,[1] David Dodoo-Arhin,[1] Kenneth I. Ozoemena,[2,3] Yury Gogotsi,[4] Alan T. Charlie Johnson,[5] and Ncholu Manyala[1,a]

[1]*Department of Physics, Institute of Applied Materials, SARChI Chair in Carbon Technology and Materials, University of Pretoria, Pretoria 0028, South Africa*
[2]*Department of Chemistry, University of Pretoria, Pretoria 0028, South Africa*
[3]*Energy Materials, Materials Science and Manufacturing, Council for Scientific and Industrial Research (CSIR), Pretoria 0001, South Africa*
[4]*Department of Materials and Engineering, and A.J Drexel Nanotechnology Institute Drexel University, 3114 Chestnut Street, PA 19104, USA*
[5]*Department of Physics and Astronomy, University of Pennsylvania, Philadelphia, Pennsylvania 19104, USA*

(Received 2 July 2013; accepted 12 August 2013; published online 21 August 2013)

We have fabricated a symmetric electrochemical capacitor with high energy and power densities based on a composite of graphene foam (GF) with ∼80 wt% of manganese oxide (MnO_2) deposited by hydrothermal synthesis. Raman spectroscopy and X-ray diffraction measurements showed the presence of nanocrystalline MnO_2 on the GF, while scanning and transmission electron microscopies showed needle-like manganese oxide coated and anchored onto the surface of graphene. Electrochemical measurements of the composite electrode gave a specific capacitance of 240 Fg^{-1} at a current density of 0.1 Ag^{-1} for symmetric supercapacitors using a two-electrode configuration. A maximum energy density of 8.3 $Whkg^{-1}$ was obtained, with power density of 20 $kWkg^{-1}$ and no capacitance loss after 1000 cycles. GF is an excellent support for pseudo-capacitive oxide materials such as MnO_2, and the composite electrode provided a high energy density due to a combination of double-layer and redox capacitance mechanisms. [http://dx.doi.org/10.1063/1.4819270]

I. INTRODUCTION

Electric double-layer capacitors (EDLCs) are charge-storage devices with a high power density, long cyclic life and low maintenance cost.[1–4] They fill the gap between batteries (high energy density) and electrolytic capacitors (high power density).[5,6] Such properties make them potentially useful for a wide range of applications such as hybrid vehicles, cordless electric tools, memory back-up, cellular phones, medical devices, military and consumer electronics.[7]

Nevertheless, the energy stored in supercapacitors (<10 $Whkg^{-1}$) is low compared to lithium ion batteries (>100 $Whkg^{-1}$). This has imposed significant challenges in employing supercapacitors as primary power source for battery replacement.[8,9] However, the performance of these devices depends on the type, properties and morphologies of the materials being used. Therefore much attention has been given to developing novel nanostructured materials with high specific surface area (SSA), controlled pore size distribution, increased operating voltage and comprehensive understanding of electrode/electrolyte interfaces at the nanoscale.[2,10–12] This led to many research

[a]Author to whom correspondence should be addressed: Electronic mail: ncholu.manyala@up.ac.za (N. Manyala)

activities focused on developing electrode materials for supercapacitors that are capable of storing more energy without sacrificing cyclic life and power density. Pseudocapacitors are energy storage devices that undergo electron transfer reactions.[13] An example of such pseudocapacitive materials is manganese oxide (MnO_2). MnO_2 has attracted much attention as an electrode material because of its multiple reversible electrochemical reactions, natural abundance, low cost, and environmental compatibility.[14–16] However, due to the low electrical conductivity of MnO_2, the rate capability and performance of MnO_2 electrodes is limited, which has hindered its potential application. The redox activity, capacitive performance and utilization of MnO_2 can be increased by adding conductive materials, such as carbon nanotubes,[17,18] conducting polymers[19,20] or graphene.[21,22] Different morphologies and shapes of the MnO_2 particles have also been reported; for example, nano-whiskers have been shown to have excellent electrochemical properties because of their large surface area.[23]

Graphene has been explored for electrochemical storage applications due to its high specific surface area, high electrical conductivity, chemical stability and excellent mechanical properties.[24,25] Graphene also offers a suitable platform for accommodating metal oxides. This is attributed to its large surface area, which allows for uniform loading and binding sites for incorporation of the metal oxide materials such as MnO_2. Also, the high conductivity of the graphene significantly improves the conductivity of the composite electrode.

Recently, Chen *et al.*[26] reported a three-dimensional (3D) flexible and conducting interconnected graphene network formed using chemical vapour deposition onto a catalytic nickel foam template. Graphene foam provides a desirable combination of a highly conductive network[27,28] and a high porosity support structure that is suitable for incorporation of nanoparticles or other fillers to occupy the pores for electrochemical applications.[29,30]

Several studies have reported on synthesis of various graphene foam/MnO_2 (GF/MnO_2) nanocomposites using chemical synthesis,[31] microwave irradiation,[32] electrodeposition,[33] redox deposition[34] and polymer-assisted chemical reduction.[35] Recently, Dong *et al.*[36] reported a simple synthesis for 3D hybrid structures of MnO_2 on graphene foam in which the morphology of the MnO_2 nanostructures was controlled by the acidity of the solution. The large specific surface area of GF ensured a large loading capacity for MnO_2 nanostructures and a large active surface area for rapid charge transfer and a large double layer capacitance. They also showed that graphene-metal oxides composites offered good adhesion for the metal oxide particles, which prevented detachment and agglomeration, thereby leading to improved capacitance in the three electrode configuration.

In this study, we report on a symmetric electrochemical capacitor fabricated using GF/MnO_2 nanostructure composite electrodes based on a nickel foam current collector. Hydrothermal synthesis of MnO_2 on graphene was performed with the goal of combining double-layer and redox capacitance for achieving high energy and power densities in one device.

II. EXPERIMENTAL SECTION

A. Synthesis of graphene foam/MnO_2 composite

Graphene foam (GF) was synthesised by chemical vapour deposition (CVD) onto a catalytic nickel foam (Alantum Innovations in Alloy Foam Munich, Germany). The detailed procedure is described in our previous report.[37] To provide mechanical support for the GF during etching of nickel, polymethylmethacrylate (PMMA) was drop coated on the sample and baked at 180 °C for 30 minutes. The samples were then placed in 3 M HCl solution at 80 °C for 5 hours to ensure that nickel was completely etched away. The resulting GF sample was placed in acetone at 50 °C for 30 minutes to remove the PMMA. The samples were then rinsed in deionised water and dried.

GF/MnO_2 composites were prepared using a hydrothermal reduction technique. Typically, 15 mg of GF was dispersed in 50 mL of 0.02 M $KMnO_4$ (Merck), and the mixture was refluxed at 150 °C for 48 hours with continuous magnetic stirring. The resultant dispersion was then centrifuged and washed several times with deionized water, and finally dried at 60 °C in an oven. All chemicals used were of analytical grade and used as received. Deionized water was used throughout the synthesis process.

B. Physical characterization of composite

Raman spectra of GF/MnO_2 composites were recorded using a WiTec-alpha 300R+ confocal Raman spectrometer (WiTec GmbH) with the laser power of 1.5 mW in order to minimize heating effects. The excitation source was a 532-nm laser through a numerical aperture of 0.9 and 100× magnification. The GF/MnO_2 composite crystal structure was characterized using powder X-ray diffraction (XRD). An XPERT-PRO diffractometer PANalytical BV, Netherlands with theta/theta geometry, operating a cobalt tube at 35 kV and 50 mA was used. The XRD patterns of all specimens were recorded in the 20.0°-80.0° 2θ range with a step size of 0.017° and a counting time of 15.240 seconds per step. Qualitative phase analysis of samples was conducted using the X'pert Highscore search match software. The surface morphology and microstructure of the composite were investigated using a Zeiss Ultra Plus 55 field emission scanning electron microscope (FE-SEM) operated at an accelerating voltage of 2.0 kV, nitrogen gas sorption analysis at 77 K (Micromeritics ASAP 2020) and transmission electron microscopy (TEM) JEOL JEM-2100F microscope operated at 200 kV. Typically, TEM samples were prepared by dispersing the samples in ethanol and dropped on lacey carbon grid for analysis.

C. Electrochemical characterization

The working electrodes for electrochemical evaluation were prepared by mixing 80 wt.% of GF/MnO_2 with 10 wt. % carbon black and 10 wt. % polyvinylidene difluoride (PVdF) binder in an agate mortar. The mixture was then dissolved in 1-methyl-2-pyrrolidinone (NMP) to form a paste. The paste was coated on the Ni foam as a current collector with a diameter of 16 mm and dried at 60 °C in an oven for 8 hours to ensure complete evaporation of the NMP.

The electrochemical test of the GF/MnO_2 electrode was performed in a three electrode configuration using glassy carbon plate as counter electrode and Ag/AgCl (3 M KCl) as the reference electrode. The symmetric GF/MnO_2/GF/MnO_2 system was investigated in a two-electrode configuration, with a glass microfiber filter paper as the separator and 1 M Na_2SO_4 solution serving as the electrolyte in both configurations. The electrochemical properties of the supercapacitor were studied using cyclic voltammetry (CV), galvanostatic charge-discharge (GV) and electrochemical impedance spectroscopy (EIS) using an Autolab PGSTAT workstation 302 (ECO-CHEMIE) driven by the general purpose electrochemical system (GPES) software.

The CV tests were carried out in the potential range of 0 to 1 V at different scan rates ranging from 5 mV/s to 100 mV/s. The galvanostatic charge-discharge measurements were also carried out at different current densities from 0.1 Ag^{-1} to 0.5 Ag^{-1} and the EIS measurements were performed in the frequency range of 100 kHz-10 mHz. The EIS data were analyzed using Nyquist plots.[1]

The cell capacitance, C_{cell}, was then calculated from the slope of galvanostatic charge-discharge curves according to the following equation

$$C_{cell} = \frac{i\,\Delta t}{\Delta v} \tag{1}$$

where i is the constant current for charge-discharge, Δt is the discharge time and Δv is the discharge voltage. The specific capacitance (per unit mass) was then calculated according to the following equation[38]

$$C_{sp} = \frac{4C_{cell}}{m} \tag{2}$$

where m is the mass of a single electrodes in the cell.

III. RESULTS AND DISCUSSIONS

Fig. 1(a) shows the Raman spectrum of the graphene foam, with prominent G and 2D peaks at 1582.2 cm^{-1} and 2705.7 cm^{-1}, respectively. The relative intensity 2D/G ratio of 1.2 and FWHM of 38.8 cm^{-1} were attributed to few layer graphene. The absence of the D-peak (disorder) at 1350 cm^{-1} showed that the graphene foam was of good quality, with a low defect density.[40] The Raman spectrum

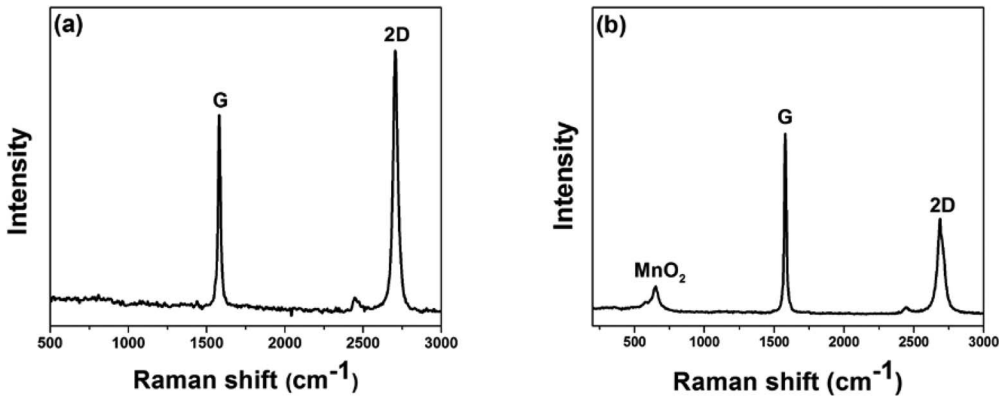

FIG. 1. Raman spectra of (a) graphene foam and (b) graphene foam/MnO_2 composite (GF/MnO_2).

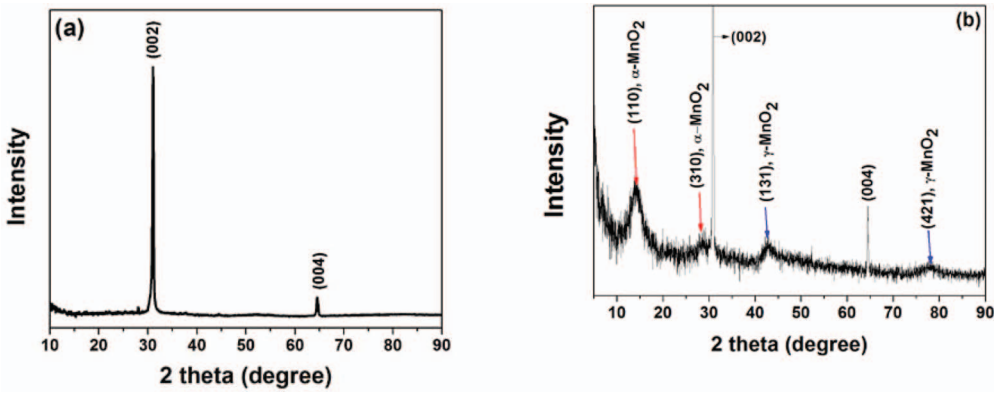

FIG. 2. XRD patterns of (a) graphene foam and (b) graphene foam/MnO_2 composite.

of the GF/MnO_2 composite (Fig. 1(b)) showed an additional sharp peak at 649.9 cm^{-1}, which was ascribed to the A_g mode arising from breathing vibrations of MnO_6 octahedral double chains. It also corresponds to the Mn-O stretching vibration mode in the basal plane of MnO_6 octahedral chains and symmetric stretching vibration Mn-O of MnO_6 groups.[41] The well-defined Raman spectrum reflects the good crystallinity of the MnO_2 in the composite. The observed reduction of the 2D/G intensity ratio after the formation MnO_2 may be due to the introduction of disorder during hydrothermal synthesis or electronic interactions between MnO_2 and GF.[42]

Both XRD patterns had narrow diffraction peaks at $2\theta = 31^\circ$ and 64.5°, which correspond to the (002) and (004) reflections of hexagonal graphite, respectively. They show that the crystalline order of the CVD-grown multi-layer graphene foam was preserved after formation of the GF/MnO_2 composite. The data for the GF/MnO_2 composite (Fig. 2(b)) showed additional diffraction peaks at $2\theta = 14.2^\circ$, 28.8°, 42.8°, and 77.7°, which are representative of α and γ phases of MnO_2. The diffraction peaks at 14.2° and 28.8° were assigned to the (110) and, (310) reflections of the α-MnO_2 phase in accordance with the ICDD PDF card No. 44-0141, while the peaks at 42.8 and 77.7 were assigned to (131) and, (421) reflections of γ-MnO_2,[43] in accordance with the ICDD PDF card No. 14-0644 respectively.

The surface area of both GF and GF/MnO_2 samples were measured using nitrogen gas sorption analysis at 77 K. Typically, the nitrogen adsorption and desorption show type II/IV isotherm as shown in Fig. 3 and the corresponding specific surface area values of 42 m^2g^{-1} and 98 m^2g^{-1} respectively.

SEM analysis showed that the nickel foam's three-dimensional (3D) porous network structure makes it an excellent template for CVD synthesis of a 3D graphene network. The SEM image of GF is shown in Fig. 4(a) after the nickel template was etched away. The GF retained the porous nature of the underlying Ni template, and therefore provided abundant surface binding sites for MnO_2

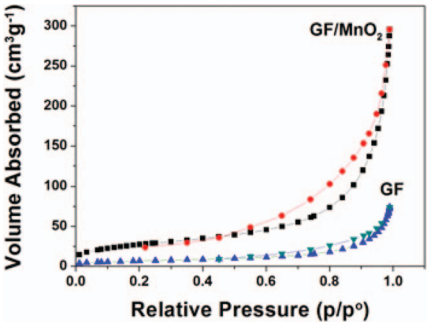

FIG. 3. Nitrogen adsorption and desorption isotherms for GF and GF/MnO_2 composite.

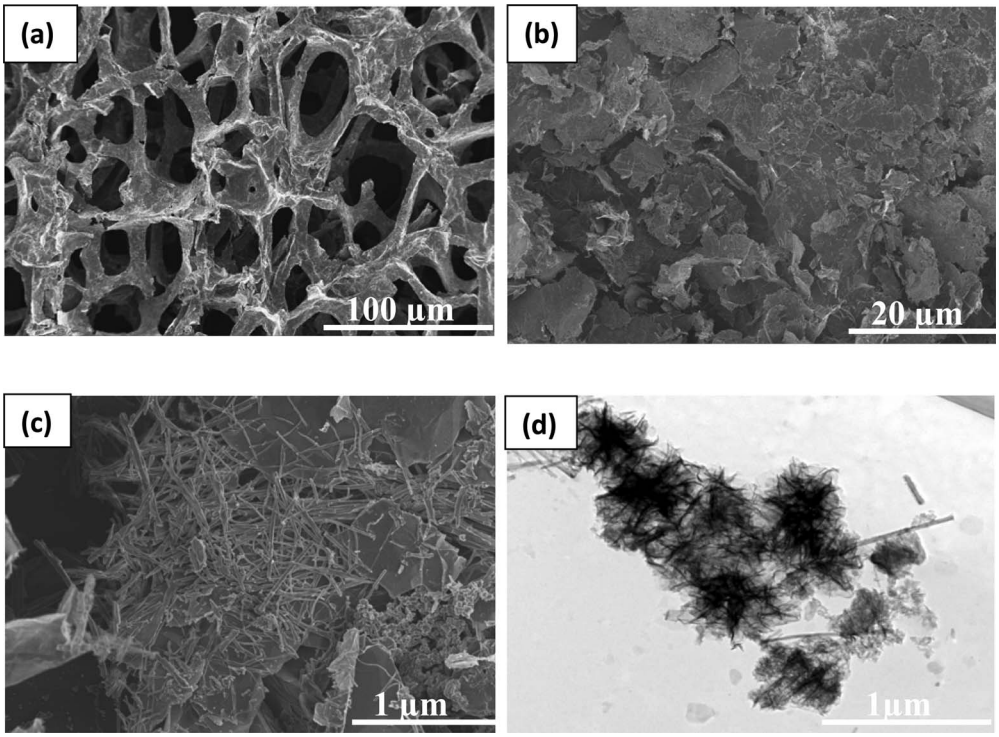

FIG. 4. SEM images of (a) graphene foam, (b, c) graphene foam/MnO_2 composite at different magnifications, and (d) TEM image of the graphene foam/MnO_2 composite.

deposition. Fig. 4(b)-4(c) are SEM images of the final GF/MnO_2 composite at different magnifications.

Fig. 4(c) reveals that most of the MnO_2 nanostructures took on a needle-like structure, which was further confirmed by transmission electron microscopy Fig. 4(d). TEM micrographs also revealed a porous, interconnected network of graphene flakes that was expected to improve the capacitive performance of the composite by enabling easy access of ions and high ionic mobility at the electrode/electrolyte interface.

Cyclic voltammetry (CV) of GF/MnO_2 electrode at different scan rates in a three electrode configuration is shown in Fig. 5(a), the CVs of the GF/MnO_2 exhibit square-like shape in a potential window of (0-1 V vs Ag/AgCl), indicating ideal capacitive performance. The galvanostatic charge-discharge curves measured at three different current densities are shown in Fig. 5(b). From these curves, the specific capacitance was calculated using equation (1). At current densities of 0.2 Ag^{-1}, 0.5 Ag^{-1} and 0.7 Ag^{-1} the calculated specific capacitance values of GF/MnO_2 electrode are 478, 341, and 266 Fg^{-1} respectively. The good capacitive performance can be attributed to

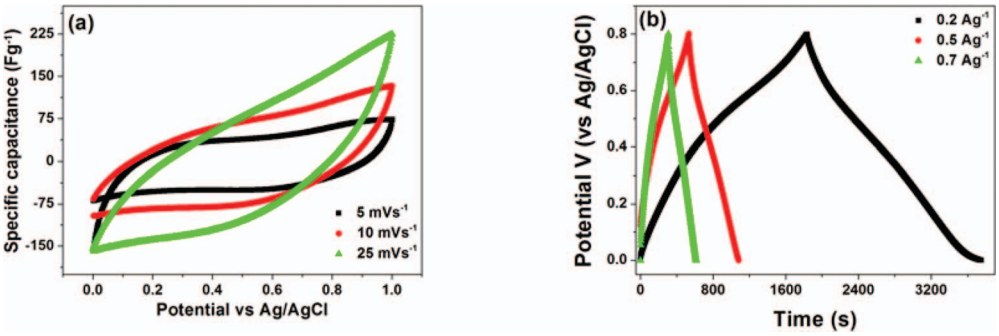

FIG. 5. (a) Cyclic voltammetry curves of GF/MnO_2 measured at 5, 10 and 25 mVs^{-1}; (b) galvanostatic charge-discharge profiles of GF/MnO_2 electrode at three different current densities in a three electrode configuration.

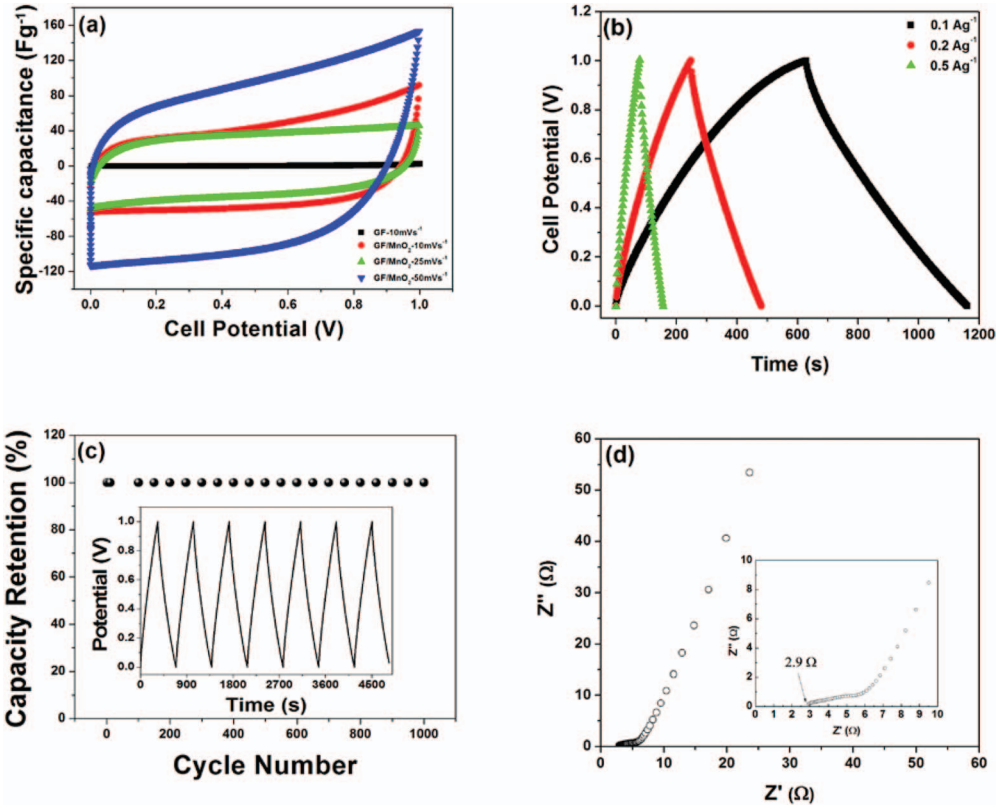

FIG. 6. Electrochemical characterizations of graphene foam/MnO_2 composites: (a) CVs of GF at scan rate of 10 mV/s and GF/MnO_2 composite at scan rates of 10, 25 and 50 mV/s; (b) the galvanostatic charge-discharge curves at three different current densities; (c) the capacity retention of the composite at a current density of 0.5 Ag^{-1}, inset shows the continuous charge-discharge curve; and (d) Nyquist plot for the GF/MnO_2 composite.

the good contact made between the MnO_2 and GF, which enhances the low-conductivity of MnO_2 needle-like structure, thus enhancing the utilization of the composite in pseudocapacitive reaction leading to rapid charge transport mechanism which results in fast dynamics and easy access to ions in electrolyte thereby reducing the diffusion resistance.

Fig. 6(a) shows the Symmetric CV of the GF at a scan rate of 10 mV/s and of the GF/MnO_2 composite at scan rates of 10 mV/s, 25 mV/s and 50 mV/s. The CV data for the GF appears as a straight line in the plot, indicating that it had a very low capacitance compared to the GF/MnO_2 composite. In contrast, the CV loops for GF/MnO_2 composite supercapacitor are nearly rectangular in shape, which is an indication of good capacitive behaviour and low contact resistance.[1] The

enhanced capacitive result is attributed to the electrochemical capacitance from MnO_2 since it is obvious that the electric double-layer capacitance from GF is very small as seen from the CV. Thus, >90% of capacitance comes from MnO_2, at least at low scan rates. CV loops expand with increasing scan rate and maintain the rectangular shape, which is a characteristic of increasing current response of the device, indicating a capacitive performance of the MnO_2 needle-like structure on GF up to 50 mV/s.

Cyclic performance of electrodes material is very important for practical applications. Galvanostatic charge-discharge measurements were performed on GF/MnO_2 composite at different current densities in the potential range from 0 to 1V and the data are presented in Fig. 6(b). It was observed that the GF/MnO_2 composite curves deviated from a linear shape, showing a contribution from redox processes. The capacitance of the cell was calculate using equation (1) while the maximum specific capacitance of the electrode material obtained using equations (2) was 240 Fg^{-1} at a current density of 0.1 Ag^{-1}, compared to 17 Fg^{-1} for the GF at the same current density. The high specific capacitance was attributed to the presence of needle-like MnO_2. The small voltage (IR) drop observed (from charge discharge curves) indicates a low internal resistance of the device, consistent with a good adhesion between the nanostructured oxide and GF surface that improved the conductivity of electrodes.

The capacitance retention as a function of cycle number is presented in Fig. 6(c). The figure shows that after 1000 cycles at a current density of 0.5 Ag^{-1}, the GF/MnO_2 composite symmetric supercapacitor device retained its initial specific capacitance. The energy storage (E) per unit mass of the GF/MnO_2 electrode and the maximum energy density of the coin cell was calculated using the equation (3) for C corresponding to C_{sp} and C_{cell} respectively. The values were found to be 34 $Whkg^{-1}$ and 8.3 $Whkg^{-1}$.

$$E = \frac{1}{2}\frac{C\,V^2}{M}, \tag{3}$$

where V is the potential window and M is the total mass of electrode material.

Fig. 6(d) shows the Nyquist plot of the GF/MnO_2 composite electrode. It is a representation of the real and imaginary parts of the impedance in the sample. The plot is divided into two regions; the high-frequency region, which is a characteristic of the charge transfer process taking place at the electrode\electrolyte interface and a straight line in the low-frequency region, which represents the electron-transfer diffusion process. The intercept at the high frequency region on the x-axis corresponds to the resistance of the electrolyte solution (R_s), and is also referred to as the equivalent series resistance (ESR) which comprises of the resistance of aqueous electrolyte, the intrinsic resistance of the composite material and the contact resistance at the electrode interface. The inset to Fig. 6(d) shows that there is no loop at high frequency that might correspond to contact resistance and the ESR value for the GF/MnO_2 composite electrode is found to be 2.9 Ω. This is a good value for composite containing 80% of poorly conducting metal oxide. This can be attributed to the good conductivity of GF.

The maximum power density (P_{max}) of the GF/MnO_2 electrodes was calculated using equation (4):

$$P_{\max} = \frac{V^2}{4MR_s} \tag{4}$$

where V is voltage applied (1 V), R_s (2.9 Ω) is the ESR, and M (4.5 mg) is the total mass of active material in the two electrodes. The maximum power density obtained for the GF/MnO_2 composite is 20 $kWkg^{-1}$.

Our symmetric (same anode and cathode) GF/MnO_2 composite supercapacitor exhibited a specific capacitance, energy density of electrode material and power density values of 240 Fg^{-1}, 34 $Whkg^{-1}$ and 20 $kWkg^{-1}$ respectively, which are comparable to the values reported by Rakhi *et al.*[39] for symmetric supercapacitors with graphene nanoplatelets-(γ-MnO_2/CNT)-nanocomposite electrodes in 1 M KOH. At the maximum voltage of 1 V they reported an electrode energy density of 43 $Whkg^{-1}$ and a power density of 26 $kWkg^{-1}$. Higher energy and power density values were reported for asymmetric devices, the voltage window for which can be extended to 2 V. For example

Fan *et al*. have reported an energy density of 51.1 Wh kg^{-1} and power density of 102.2 Wkg^{-1} for an asymmetric supercapacitor using a graphene/MnO_2 composite as a positive electrode and activated carbon nanofibers as a negative electrode in a neutral aqueous Na_2SO_4 electrolyte,[45] while Choi *et al*. reported values of 44 $Whkg^{-1}$ and 25 $kWkg^{-1}$ for energy and power densities of asymmetric supercapacitor device of chemically modified graphene e-CMG/e-CMG-MnO_2 composite.[44] Our results in the symmetric configuration with the maximum voltage window of 1 V give values that are comparable to those obtained in the asymmetric configuration. Therefore, GF with hydrothermally deposited MnO_2 needles-like structure is a promising candidate for capacitive energy storage.

IV. CONCLUSIONS

Graphene foam/MnO_2 composite electrodes have been fabricated by hydrothermal deposition of MnO_2 from $KMnO_4$, and their electrochemical properties have been tested in a symmetric device with Na_2SO_4 as the electrolyte. The 3D porous network structure of GF allows for a uniform coating and high loading of α- and γ-MnO_2 needle-like structures. The composite exhibits a specific capacitance of 240 Fg^{-1} at a current density of 0.1 Ag^{-1} and no change in capacitance was observed after 1000 cycles at a current density of 0.5 Ag^{-1}. The composite electrodes exhibited energy and power densities of 34 $Whkg^{-1}$ and 20 $kWkg^{-1}$ respectively, which are among the highest values reported so far for symmetric two-electrode cells. The results obtained here indicate that graphene foam/MnO_2 composites are promising for electrochemical applications.

ACKNOWLEDGMENTS

This work is based upon research supported by the South African Research Chairs Initiative of the Department of Science and Technology (DST) and the National Research Foundation (NRF). Any opinion, findings and conclusions or recommendations expressed in this work are those of authors and therefore the NRF and DST do not accept any liability with regard thereto. A.T.C.J acknowledges support from the LRSM, through the U.S. National Science Foundation MRSEC, Grant No. DMR-1120901. Y.G. was supported by the US Department of Energy, Energy Storage Systems Research Program through Sandia National Laboratory. A. B. acknowledges the financial support from University of Pretoria for his study from both Energy Institutional research theme (IRT) and PhD bursary scheme.

[1] B. E. Conway, Electrochemical Supercapacitors Scientific Fundamentals and Technological Applications 1999.
[2] P. Simon and Y. Gogotsi, "Capacitive Energy Storage in Nanostructured Carbon–Electrolyte Systems," Acc. Chem. Res. **46**, 1094–1103 (2012).
[3] J. Miller and A. Burke, "Electrochemical capacitors: challenges and opportunities for real-world applications," Electrochem. Soc. Inter. **17**, 53–57 (2008).
[4] A. S. Aricò, P. Bruce, B. Scrosati, J.-M. Tarascon, and W. Van Schalkwijk, "Nanostructured materials for advanced energy conversion and storage devices," Nat. Mater. **4**, 366–77 (2005).
[5] R. Kötz, "Principles and applications of electrochemical capacitors," Electrochim. Acta **45**, 2483–2498 (2000).
[6] X. Zhao, B. M. Sánchez, P. J. Dobson, and P. S. Grant, "The role of nanomaterials in redox-based supercapacitors for next generation energy storage devices," Nanoscale **3**, 839–55 (2011).
[7] P. J Hall, M. Mirzaeian, S. I. Fletcher, F. B. Sillars, A. J. R. Rennie, G. O. Shitta-Bey, G. Wilson, A. Crude, and R. Carter, "Energy storage in electrochemical capacitors: Designing functional materials to improve performance," Energy Environ. Sci. **3**, 1238–1251 (2010).
[8] A. Burke, "R&D considerations for the performance and application of electrochemical capacitors," Electrochim. Acta **53**, 1083–1091 (2007).
[9] E. Frackowiak and F. Béguin, "Carbon materials for the electrochemical storage of energy in capacitors," Carbon **39**, 937–950 (2001).
[10] S. W Lee, B. M. Gallant, H. R. Byon, P. T Hammond, and Y. Shao-Horn, "Nanostructured carbon-based electrodes: bridging the gap between thin-film lithium-ion batteries and electrochemical capacitors," Energy Environ. Sci. **4**, 1972–1985 (2011).
[11] L. L. Zhang, R. Zhou, and X. S. Zhao, "Graphene-based materials as supercapacitor electrodes," J. Mater. Chem. **20**, 5983–5992 (2010).
[12] F. Du, D. Yu, L. Dai, S. Ganguli, V. Varshney, and A. K. Roy, "Preparation of Tunable 3D Pillared Carbon Nanotube–Graphene Networks for High-Performance Capacitance," Chem. Mater. **23**, 4810–4816 (2011).
[13] J. R. Millerand and P. Simon, "Materials science. Electrochemical capacitors for energy management," Science **321**, 651–2 (2008).

[14] W. Wei, X. Cui, W. Chen, and D. G. Ivey, "Manganese oxide-based materials as electrochemical supercapacitor electrodes," Chem. Soc. rev. **40**, 1697–721 (2011).
[15] J. Liu, J. Essner, and J. Li, "Hybrid Supercapacitor Based on Coaxially Coated Manganese Oxide on Vertically Aligned Carbon Nanofiber Arrays," Chem. Mater. **22**, 5022–5030 (2010).
[16] C.-Y. Chen, C.-Y. Fan, M.-T. Lee, and J.-K. Chang, "Tightly connected MnO_2–graphene with tunable energy density and power density for supercapacitor applications," J. Mater. Chem. **22**, 7697–7700 (2012).
[17] M. Sang-Bok, N. Kyung-Wan, Y. Won-Sub, Y. Xiao-Qing, A. Kyun-Young, O. Ki-Hwan, and K. Kwang-Bum, "Electrochemical properties of manganese oxide coated onto carbon nanotubes for energy-storage applications," J. Power Sources **178**, 483–489 (2008).
[18] A. E. Fischer, K. A. Pettigrew, D. R. Rolison, R. M. Stroud, and J. W Long, "Incorporation of homogeneous, nanoscale MnO_2 within ultraporous carbon structures via self-limiting electroless deposition: Implications for electrochemical capacitors," Nano lett. **7**, 281–286 (2007).
[19] R. I. Jafri, A. K Mishra, and S. Ramaprabhu, "Polyaniline–MnO_2 nanotube hybrid nanocomposite as supercapacitor electrode material in acidic electrolyte," J. Mater. Chem. **21**, 17601–17605 (2011).
[20] J. Kim, K. H. Lee, L. J. Overzet, and G. S. Lee, "Synthesis and Electrochemical Properties of Spin-Capable Carbon Nanotube Sheet/MnO," Nano Lett. **11**, 2611–2617 (2011).
[21] H. Wang, C. Li-Feng, Y. Yang, H. S. Casalongue, J. T. Robinson, Y. Liang, Y. Cui, and H. Dai, "Mn_3O_4 -Graphene Hybrid as a High Capacity Anode Material for Lithium Ion Batteries," J. Am. Chem. Soc. **132**, 13978–13980 (2010).
[22] J. Zhu and J He, "Facile synthesis of graphene-wrapped honeycomb MnO2 nanospheres and their application in supercapacitors," ACS appl. mater. interfaces **4**, 1770–1776 (2012).
[23] L. Li, Z.-Y. Qin, L.-F. Wang, H.-J. Liu, and M.-F Zhu, "Anchoring alpha-manganese oxide nanocrystallites on multi-walled carbon nanotubes as electrode materials for supercapacitor," J. Nanoparticle Res. **12**, 2349–2353 (2010).
[24] M. D. Stoller, S. Park, Y. Zhu, J An, and R. S. Ruoff, "Graphene-based ultracapacitors," Nano lett. **8**, 3498–3502 (2008).
[25] Y. Wang, Z. Q. Shi, Y. Huang, Y. Ma, C. Wang, M. Chen, and Y Chen, "Supercapacitor Devices Based on Graphene Materials," J. Phy. Chem. C **113**, 13103–13107 (2009).
[26] Z. Chen, W. Ren, L. Gao, B. Liu, S. Pei, and H-M Cheng, "Three-dimensional flexible and conductive interconnected graphene networks grown by chemical vapour deposition," Nat. mater. **10**, 424–428 (2011).
[27] Y. Chen, X. Zhang, P. Yu, and Y Ma, "Electrophoretic deposition of graphene nanosheets on nickel foams for electrochemical capacitors," J. Power Sources **195**, 3031–3035 (2010).
[28] H. Ji, L. Zhang, M. Pettes, H Li, and S. Chen, "Ultrathin graphite foam: A three-dimensional conductive network for battery electrodes," Nano lett. **12**, 2446−2451 (2012).
[29] X. Huang, X Qi, F. Boey, and H. Zhang, "Graphene-based composites," Chem. Soc. rev. **41**, 666–686 (2012).
[30] Y. Xu, X. Huang, Z. Lin, X. Zhong, Y. Huang, and X. Duan, "One-step strategy to graphene/$Ni(OH)_2$ composite hydrogels as advanced three-dimensional supercapacitor electrode materials," Nano Res. **6**, 65–76 (2012).
[31] S. Chen, J. Zhu, X. Wu, Q. Han, and X. Wang, "Graphene oxide−MnO_2 nanocomposites for supercapacitors," Acs Nano **4**, 2822–2830 (2010).
[32] J. Yan, Z. Fan, T. Wei, W. Qian, M. Zhang, and F. Wei, "Fast and reversible surface redox reaction of graphene–MnO_2 composites as supercapacitor electrodes," Carbon **48**, 3825–3833 (2010).
[33] Q. Cheng, J. Tang, J. Maa, H. Zhanga, N. Shinyaa, and L-C. Qinc, "Graphene and nanostructured MnO_2 composite electrodes for supercapacitors," Carbon **49**, 2917–2925 (2011).
[34] Z. Li, J. Wang, S. Liu, X. Liu, and S. Yang, "Synthesis of hydrothermally reduced graphene/MnO_2 composites and their electrochemical properties as supercapacitors," J. Power Sources **196**, 8160–8165 (2011).
[35] Y. Qian, S. Lu, and F. Gao, "Preparation of MnO_2/graphene composite as electrode material for supercapacitors," J. Mater. Sci. **46**, 3517–3522 (2011).
[36] X. Dong, X. Wang, J. Wang, H. Song, X. Li, L. Wang, M. B. Chan-Park, C. M. Li, and P. Chen, "Synthesis of a MnO_2–graphene foam hybrid with controlled MnO_2 particle shape and its use as a supercapacitor electrode," Carbon **50**, 4865–4870 (2012).
[37] A. Bello, K. Makgopa, M Fabiane, D. Dodoo-Ahrin, K. I. Ozoemena, and N. Manyala, "Chemical adsorption of NiO nanostructures on nickel foam-graphene for supercapacitor applications," J. Mat. Sci. (2013).
[38] M. D. Stoller and Rodney S. Ruoff, "Best practice methods for determining an electrode material's performance for ultracapacitors," Energy Environ. Sci. **3**, 1294–1301 (2010).
[39] R. B. Rakhi, W. Chen, D Cha, and H. N. Alshareef, "Nanostructured Ternary Electrodes for Energy-Storage Applications," Adv. Energy Mater. **2**, 381–389 (2012).
[40] A. C. Ferrari, "Raman spectroscopy of graphene and graphite: disorder, electron–phonon coupling, doping and nonadiabatic effects," Solid State Comm. **143**, 47–57 (2007).
[41] T. Gao, H. Fjellvåg, and P. A Norby, "comparison study on Raman scattering properties of α- and β-MnO_2," Analytica Chim. Acta **648**, 235–239 (2009).
[42] Z. Ni, T. Yu, Z. Luo, Y. Wang, and L. Liu, "Probing charged impurities in suspended graphene using Raman spectroscopy," ACS Nano **3**, 569–574 (2009).
[43] L. Chen, L-J. Sun, F. Luan, Y. Liang, Y. Li, and X-X Liu, "Synthesis and pseudocapacitive studies of composite films of polyaniline and manganese oxide nanoparticles," J. Power Sources **195**, 3742–3747 (2010).
[44] Z. Fan, J. Yan, T. Wei, L. Zhi, G. Q. Ning, T. Y. Li, and F. Wei, "Asymmetric Supercapacitors Based on Graphene/MnO_2 and Activated Carbon Nanofiber Electrodes with High Power and Energy Density," Adv. Funct. Mater. **21**, 2366–2375 (2011).
[45] B. G. Choi, M. Yang, W. H. Hong, J. W. Choi, and Y. S. Huh, "3D macroporous graphene frameworks for supercapacitors with high energy and power densities," ACS nano **6**, 4020–8 (2012).